

Relations between stress drops and acoustic emission measured during mechanical loading

Noam Zreihan,¹ Eilon Faran,¹ Eduard Vives,² Antoni Planes,² and Doron Shilo¹

¹*Department of Mechanical Engineering, Technion, Haifa 32000, Israel*

²*Departament de Física de la Matèria Condensada, Facultat de Física, Universitat de Barcelona, Diagonal 645, 08028 Barcelona, Catalonia, Spain*



(Received 2 July 2018; revised manuscript received 10 February 2019; published 11 April 2019)

Avalanche events occur during mechanical loading of many material systems and are characterized by stress drops and acoustic emission (AE). Stress drops are directly related to the macroscopic response of the investigated material, but their detection capability is restricted to relatively large and slow events. AE measurements can detect events with smaller amplitude and shorter duration, but their energy and duration are not directly related to the change of the system. In this paper, we present simultaneous measurements of stress drops and AE during mechanically induced twin boundary motion in Ni-Mn-Ga. We found that the probability of finding an AE event during a stress drop is ~ 100 times higher than between stress drops. Analysis of the relations between mechanical energy drops ΔU_m and acoustic emitted energy E_{AE} , on the level of individual events, reveals the existence of a lower bound for E_{AE} , which is approximately proportional to ΔU_m . These results imply that the macroscopic stress changes generate acoustic waves, which contribute a well-defined amount of energy that is equal to the lower bound function. Furthermore, smaller scale events that are related to microscopic subprocesses by which the twin boundary moves generate additional AE energy. The latter contribution displays a power-law distribution, which implies that these processes are close to criticality.

DOI: [10.1103/PhysRevMaterials.3.043603](https://doi.org/10.1103/PhysRevMaterials.3.043603)

I. INTRODUCTION

Numerous materials, including granular materials [1], glasses [2,3], ferroic materials [4], shape memory alloy [5], and mineral rocks [6,7], respond to smooth mechanical loading through discrete impulsive events called avalanches [8,9]. This phenomenon was widely studied in relation to instabilities of plastic flow in alloys, known as the Portevin–Le Chatelier effect [10]. The statistical study of the characteristic properties of avalanche events reveals important information about the mechanisms of the mechanical response and the physics of the studied system. For example, in many cases, the statistical distribution of avalanche amplitudes, energies, or durations reveals a power-law distribution that spans several orders of magnitudes [8,11]. This behavior indicates that the system evolves in a dynamic critical state [12–15].

There are two types of experimental methods for studying avalanche events. The first is based on measurements of a variable, such as the force [3,16–20], the corresponding displacement [21], or the heat (or enthalpy) involved in the process [15,22], which are directly related to the overall (macroscopic) response of the investigated material. These measurements allow evaluating the energy released by the event [16,23], the displacement of a moving twin/phase boundary during the event [16,17], and the volume of the material that underwent a transformation during the event [23]. Because these methods measure macroscopic changes of the system, their detection capabilities are constrained to relatively large discrete events or many consecutive overlapped microscopic events with a limited temporal resolution [23]. One should also take into account the influence of the external noise and the interaction between the sample and the measurement device.

The second type of experimental methods is based on measurements of local microscopic events that are associated with the process through which the material responds. The most common method of this type is the measurement of acoustically emitted waves that are generated by rapid changes of the local strain field that occur during the avalanche event [8,9,11]. These measurements are much more sensitive than macroscopic ones and are capable of detecting events with an energy down to 1 aJ and below [2,5]. Thus, acoustic emission (AE) measurements may provide information on the mechanism by which the avalanche proceeds.

To reduce noise effects, AE measurements are commonly limited to a relatively narrow frequency range, typically between 100 kHz and 3 MHz [24]. This frequency range corresponds to excitations duration τ in the range of 0.3–10 μ s. The acoustic waves travel back and forth along the sample and generate echoes in the transducer. The decay time of the acoustic signal often lasts more than ~ 100 μ s (in general this time is bounded by the hit detection time that in our case was fixed to 200 μ s), during which more AE excitations may occur. Thus, a single AE detected event may be composed of several excitation events, as shown in Fig. 1.

The relationship between the information provided by the two aforementioned types of experimental methods is at present not clear. The complexity of the problem is demonstrated in Fig. 1, which shows a typical AE signal and force drop event that have been measured simultaneously. The AE signal displays several excitations that occur at the microsecond timescale and cannot be captured by the force sensing system. On the other hand, the overall force drop event occurs on the millisecond timescale. Therefore, it is expected to generate a wide band of acoustic waves, starting at a frequency

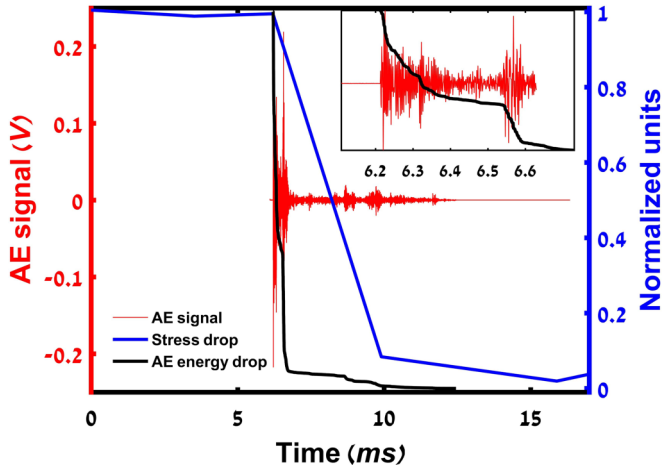


FIG. 1. A typical AE signal (left axis) and force drop (normalized, right axis) measured during uniaxial compression of a Ni-Mn-Ga single crystal. The curve of the AE energy drop (black line, right axis) is calculated by integrating the square of the AE signal (red line) and normalizing via $1 - E(t)/E_{\text{tot}}$, where $E(t)$ is the emitted energy up to time t and E_{tot} is the overall emitted energy during this signal. The inset shows the beginning of the AE signal and demonstrates that it is generated by several separated excitations.

in the subkilohertz range, which is much below the detectable range of AE measurement systems. Thus, the measured AE signal captures only a small fraction of the overall acoustic energy that is emitted during the force drop event.

The above discussion indicates that force measurements capture macroscopic changes in the system, but miss small/short-time microscopic events. On the other hand, AE measurements are very sensitive to short-time microscopic changes, but their output is strongly influenced by the sample size and geometry, the transmission function of the AE transducer, and the bandwidth of the analog filter. As a result, AE characteristics, such as the amplitude, the overall energy, and the duration, are not directly related to the change of the system. It is therefore important to understand the relationship between avalanche sizes measured by AE and macroscopic changes of the system, expressed, for example, by force drops.

The relation between stress drops and emitted elastic waves is a long-standing problem in seismology [25–28]. There are significant differences between seismic avalanches and avalanches that are generated during laboratory mechanical tests. For example, the “sample size” and the frequency of the measured elastic waves differ by many orders of magnitude. Nevertheless, some results are common to both types of avalanches, e.g., the common power-law distribution of several avalanche parameters [8,9,26].

Several concepts that are used in seismology studies are relevant also for avalanches that are generated by phase or twinning transformation in much smaller samples. For example, in both cases, the source for the avalanche has units of volume. The source for seismic avalanches is characterized by the product $\bar{D} \cdot S$, where \bar{D} is the average slip displacement over the fault and S is the fault area [26,27]. Measured variables, such as the seismic moment $M_0 = \mu \bar{D} \cdot S$ (where μ is the shear modulus), are directly related to $\bar{D} \cdot S$ [26,27].

Therefore, $\bar{D} \cdot S$ is the main source for the variability of avalanche sizes. The source for avalanches that are generated by phase or twinning transformation is characterized by the product $\varepsilon_T \cdot \Delta V$, where ε_T is the transformation/twinning strain and ΔV is the volume that experienced phase/twinning transformation during the avalanche event. The macroscopic stress drop during such avalanches is approximately given by $\Delta\sigma \cong \frac{Y\varepsilon_T \cdot \Delta V}{V}$, where V is the sample’s volume and Y is an effective elastic modulus related to the stiffness of the sample and the loading machine [16,23]. The volume ΔV may vary over several orders of magnitude and is the main source for the variability of $\Delta\sigma$.

In seismology, the stress drop $\Delta\sigma_{\text{fault}}$ relates to the stress at the source of the avalanche, i.e., at the fault [26,27], rather than the average stress $\Delta\sigma$ in the sample. For most earthquakes, $\Delta\sigma_{\text{fault}}$ is nearly constant (may vary up to one order of magnitude) and reflects a material property [26,27]. The overall energy of the radiated seismic waves is roughly given by $E_R \approx \frac{1}{2} \Delta\sigma_{\text{fault}} \bar{D} \cdot S$ [26,27]. Because $\Delta\sigma_{\text{fault}}$ is approximately constant, the distribution of E_R is mainly attributed to the distribution of the source of the avalanche $\bar{D} \cdot S$ and E_R roughly scales as $E_R \sim M_0$ [26,27].

Another difference between seismology and laboratory tests involving the measurements of AE signal relates to the bandwidth of the sensors. Seismic sensors have a bandwidth of approximately three decades that is designed to capture most of the spectrum of the emitted waves. Thus the measured E_R represents a significant part of the overall radiated energy [26]. In contrast, “broadband” AE transducers capture a frequency range of less than a decade. As a result, the measured AE energy E_{AE} represents a small fraction of the overall radiated acoustic energy. This fraction is governed by the excitation duration τ that determines the spectrum of the emitted waves. Thus, the distribution of E_{AE} is affected both by the distribution of the avalanche source $\varepsilon_T \cdot \Delta V$ and by the distribution of τ . This apparent drawback enables AE to be very sensitive to small (microscopic) events that occur during short duration τ .

In previous studies of the relations between stress drops and AE during mechanical tests the durations of stress drops were in the *seconds* timescale while the durations of AE events were in the *milliseconds* timescale. Therefore, the correlation between stress drops and AE events has not been analyzed on the level of individual stress drop event vs individual AE event. For example, Lebyodkin and coworkers [18–20] performed tensile tests on Al-Mg alloy and reported the presence of numerous AE events during each measured stress drop. They presented cross-correlations between the time derivative of the stress and several AE characteristics during intervals of 0.5 s. Navas-Portella *et al.* [2] have recently studied the compression of a porous glass (Vycor) and analyzed the correlation between force drops and the sum of acoustic energy emitted during given time intervals of 0.1 s. Their results show that most of the time intervals did not contain a detectable force drop, but contained more than one AE event. A Pearson correlation coefficient of $R \approx 0.6$ was found, indicating a clear positive correlation. However, for the same force change, the measured values of AE energies were scattered over –three to six orders of magnitude. The reason for the large scattering of AE data has yet to be resolved.

In the present paper, we performed simultaneous measurements of stress drops and AE during mechanical loading of a single Ni-Mn-Ga crystal. In this material, avalanche events are induced by a jerky motion of a single twin boundary [16,29]. The force was measured by a piezoelectric sensor with high resolution and bandwidth that enabled detecting stress drops with a duration of a few milliseconds. Thus, the durations of individual stress drops and AE events were on the same timescale (see, e.g., Fig. 1). These conditions allowed us to identify a single dominant AE signal that was emitted during each stress drop event. An analysis of the relationship between stress drops and dominant AE signals, on the level of individual events, revealed a good correlation between the stress drop and a lower bound for the energy of the AE signal. We suggest an explanation, according to which the lower bound AE energy is associated with the macroscopic stress changes. An additional contribution to the AE energy is generated by local microscopic events, such as the overcoming of energy barriers for twin boundary motion.

II. EXPERIMENTAL METHODS

The investigated sample was a single crystal of the ferromagnetic shape memory alloy, Ni-Mn-Ga, produced by AdaptaMat, Ltd. The sample had a cuboid shape with dimensions $20.0 \times 2.3 \times 3.0 \text{ mm}^3$. Measurements were performed at room temperature, at which this alloy is in the martensitic phase and has a monoclinic 10M modulated structure. The latter is nearly tetragonal, with minor monoclinic distortion [30]. Due to this distortion, Ni-Mn-Ga has two types of twins, I and II, that are different in their crystallographic orientations [31,32] and dynamic properties [33–35]. The faces of the studied crystals were parallel to the $\{100\}$ planes of the parent cubic austenite phase. In this crystal orientation, the projection of type-I boundaries on the top surface is parallel to the $[100]$ direction while the projection of type-II boundaries forms an angle of approximately 6° with the $[100]$ direction [11,36]. Optical observations indicated that only type-I twin boundaries propagated at the martensite phase in the tested crystal. In addition, optical videos indicated that during any given time interval only a single twin boundary propagated in the examined sample.

The twinning stress for the motion of type-I twin boundaries in Ni-Mn-Ga is approximately 1 MPa (see Fig. 2), while the yield stress for ordinary dislocation glide is higher than 100 MPa. Except for twinning reorientation, Ni-Mn-Ga is often subjected to 180° magnetic domain switching. However, this process is not associated with a strain change and therefore is not expected to produce AE or stress drops. Thus, the source for AE and stress drops in the studied samples is solely the motion of a single twin boundary.

Force and AE measurements were performed simultaneously, using displacement-driven mechanical test machine SMART.PRO (Zwick/Roell). Compression tests were performed along the long axis of the crystal at a constant bridge speed of $c = 0.03 \text{ mm/min}$ that corresponds to an average twin boundary velocity of $\bar{v}_{\text{TB}} = c/\varepsilon_T = 8.3 \times 10^{-6} \text{ m/s}$ (where $\varepsilon_T = 0.06$ is the twinning strain that is determined by the lattice parameters of the crystal [37]). The load was

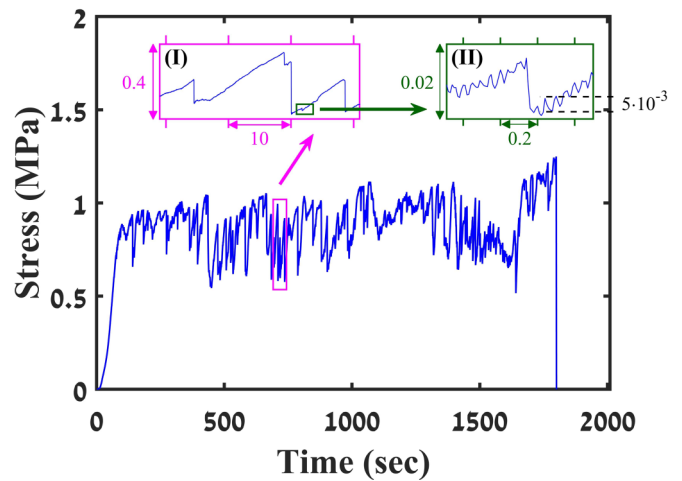


FIG. 2. A typical stress vs time profile. Inset I zooms in on a time interval of 32 s, displaying several stress drops with a large variety of magnitudes. Inset II zooms in on a time interval of 0.8 s, displaying a single stress drop superimposed on the background fluctuations.

measured using a piezoelectric force sensor, Kistler 9215, with a 1-mN resolution and natural frequency of 50 kHz. The stiffness of the experimental system elements (i.e., the loading frame bridge, mechanical adaptors, and the force sensor) is larger by several orders of magnitude than that of the tested sample.

AE signals were measured by a broadband piezoelectric transducer, with a frequency range between 200 kHz and 1 MHz, that was placed in the loading frame punch. The electric signals from the AE transducer were preamplified (60 dB), analog band filtered between 100 kHz and 3 MHz, and analyzed by a PCI-2 acquisition system (Euro Physical Acoustics, Mistras Group) working at 40 MHz. The acquisition system is programmed to record at the time when the amplified signal $V(t)$ crosses a fixed threshold of 23 dB, and ends when the signal remains below the threshold for more than $200 \mu\text{s}$. The energy of each signal was calculated as the integral of $V^2(t)$ over the duration of the event, divided by a reference resistance of $10 \text{ k}\Omega$ (see Refs. [2,24]).

The PCI-2 system acquires the value of the force from the Kistler 9215 sensor simultaneously through two procedures: (a) in regular intervals every 10 ms and (b) every time that an AE signal is detected when the voltage crosses the threshold. Because stress drops were accompanied with AE signals (see section D of the Results), the measured duration of most of the stress drops was shorter than 10 ms (see the example in Fig. 1, in which the duration of the force drop is approximately 3 ms). Yet, it is expected that in some cases the real duration of the stress drop is shorter than the captured duration.

The source of the emitted waves is much smaller than the sample length L , for both the microscopic and macroscopic events. The long and thin geometry of the sample implies that far from the source of the emitted waves, i.e., at a distance larger than the thickness of the sample but smaller than the length of the sample, the wave fronts become approximately planar. Then, the planar acoustic waves travel back and forth along the length of the sample dozens of times before the acoustic energy decays.

The velocity of acoustic waves in Ni-Mn-Ga is approximately 4200 m/s [38,39]. Thus, the time that is required for the acoustic waves to travel along the entire sample length (20 mm) is approximately 5 μ s. This time is much shorter than the decay time of AE signals (larger than 100 μ s). Under these conditions, the location of the source of the AE within the sample has a minor effect on the overall (integrated) AE energy of the signal. In addition, the AE sensor covers the full upper face of the sample, thus it catches almost 50% of the AE energy.

III. RESULTS

A. Identification of stress drops

Figure 2 shows a typical stress vs time measurement. When the stress reaches a threshold value, known as the twinning stress, the twin boundary starts moving in a jerky manner that results in the observed serration pattern. A zoom-in on a short time interval (inset I in Fig. 2) shows that the serrations are composed of relatively long time intervals during which the stress gradually increases, followed by short time intervals during which the stress decreases sharply. This pattern has been observed during the motion of type-I twin boundaries in Ni-Mn-Ga [16] and is significantly different from the pattern that is detected during the motion of type-II twin boundaries in the same material [29]. The stress drop events are caused by a rapid motion of the twin boundary [16]. Inset I also shows the large variety in the magnitude of the stress drops.

Inset II in Fig. 2 shows a zoom-in on a single stress drop event, which is relatively small (0.016 MPa) but still detectable. At the stress and timescales shown in inset II, it is possible to observe fluctuations in the stress signal with a peak-to-peak amplitude of 5×10^{-3} MPa and a time period of approximately 50 ms. These fluctuations were caused by low-frequency vibrations of the loading machine and can be considered as part of the measurement noise. Note that compared with the period of this vibration the stress drop observed in inset II, as well as all other stress drops, occurred at a much shorter timescale of a few milliseconds.

In accordance with the aforementioned observations, we defined stress drop as events during which the stress decreased by more than 0.01 MPa (twice the peak-to-peak noise vibrations) within less than 10 ms (five times shorter than the time period of the noise vibrations). In a few rare cases, the stress continued to decrease by more than 0.01 MPa during the next 10 ms. In such cases, we considered the stress drop as the merge of the two drops.

B. Distributions of acoustic emission energy

Figure 3 presents the complementary cumulative distribution functions (CCDFs) of the AE energy E_{AE} , corresponding to the whole set of 177305 detected avalanche events. The linear part of the curve, in a log-log plot, indicates a power-law distribution over five decades of E_{AE} . The data presented in Fig. 3 can be fitted to a probability density function (PDF) of the form

$$P(E_{AE}) \sim E_{AE}^{-\varepsilon} \exp\left[-\frac{E_{AE}}{E_{cutoff}}\right] \quad (1)$$

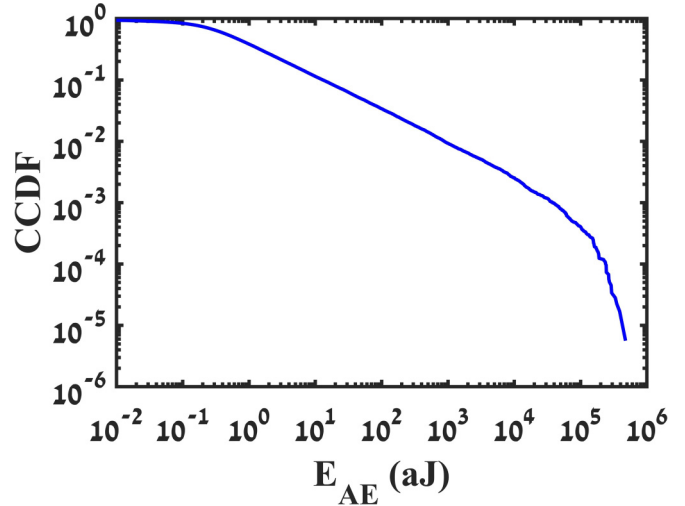


FIG. 3. CCDF of acoustic emitted energy during 177305 avalanche events.

where ε is the exponent of the power law and $E_{AE,cutoff}$ is a cutoff value above which the probability distribution deviates from the power law. By applying the maximum likelihood (ML) method [36,40,41], we obtained, $\varepsilon = 1.50 \pm 0.005$ and $E_{AE,cutoff} = 2 \times 10^5 \pm 0.94 \times 10^5$ aJ. The same value of ε was obtained for energy distributions of AE events measured during the motion of type-II twin boundaries in Ni-Mn-Ga, but the cutoff energy $E_{AE,cutoff}$ was smaller in that case by two orders of magnitude [29].

C. Distributions of mechanical energy drops

The macroscopic mechanical energy that is released during the stress drop is given by

$$\Delta U_m = \frac{F_{up}^2 - F_{down}^2}{2k} \quad (2)$$

where k is the effective stiffness of the sample and the loading machine and F_{up} and F_{down} are the force values before and after the stress drop, respectively. Equation (2) is obtained by recognizing that the displacement applied by the loading machine during the short time of stress drop is negligible.

The CCDF of all mechanical energy drops ΔU_m (325 events) is presented by the blue curve in Fig. 4. The distribution of ΔU_m fits the distribution function given by Eq. (1) (black dashed curve) only in a range of $0.6 < \Delta U_m < 3 \mu$ J. In the range of larger ΔU_m values, when $\Delta U_m > 4 \mu$ J, the measured distribution fits a normal distribution (magenta curve). A linear combination of these two distributions (red dashed curve) fits quite well the actual distribution over the entire range.

A previous study of stress drop distributions during type-I twin boundary motion in a single Ni-Mn-Ga crystal displayed a log-normal distribution with a characteristic (most probable) value that is approximately related to the mean value of the normal distribution presented in Fig. 4 [16]. The additional power-law contribution at small ΔU_m values may occur due to the higher resolution of the force sensor used in the present paper. The exact values of the power-law

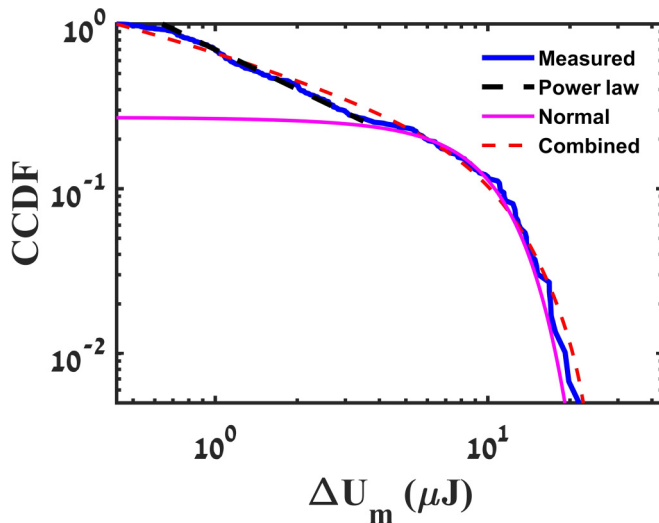


FIG. 4. CCDF of the measured mechanical energy drops (blue solid line). The distribution can be described by a combination of a power law (black dashed line) and normal distributions (magenta solid line), which is illustrated by the red dashed line.

exponent (approximately 1.8) and the mean of the normal distribution (approximately $9\mu\text{J}$) are hard to determine with strong statistical confidence. These values are not crucial for the analysis of the correlation between stress drops and AE energy that is presented in the next section.

D. Relations between stress drops and AE signals

This section starts with the identification of AE signals that were emitted during each stress drop. AE signals that began slightly before the stress drop but ended during the stress drop have also been accounted for. We considered AE signals with an energy larger than 10 aJ, because signals with smaller energies are very abundant (approximately 89% of all AE signals according to Fig. 3) and are not necessarily related to a stress drop, even if they are emitted during the stress drop. In most of the cases, there was a single AE signal during a stress drop. In cases where there were more AE signals, one was dominant and the others were smaller by several orders of magnitude. Thus, we were able to associate a single AE signal with an energy larger than 10 aJ to almost all individual stress drops.

The aforementioned procedure provided the following results.

(1) 94% (305 out of 325) of the stress drop events were accompanied by an AE signal with an energy larger than 10 aJ. For comparison, based on all AE events, the probability of finding an AE event during an arbitrary time interval of 10 ms (longer than a typical stress drop) is 0.6%. Thus, the probability of finding an AE event is much larger during a stress drop than between stress drops.

(2) 98.5% (19937 out of 20242) of the AE signals with an energy larger than 10 aJ were not associated with any detectable stress drop event. It is possible that these AE signals are still associated with small stress drops that are below the detection capability of our force sensor. In particular, it is possible that these AE signals occur due to local microscale

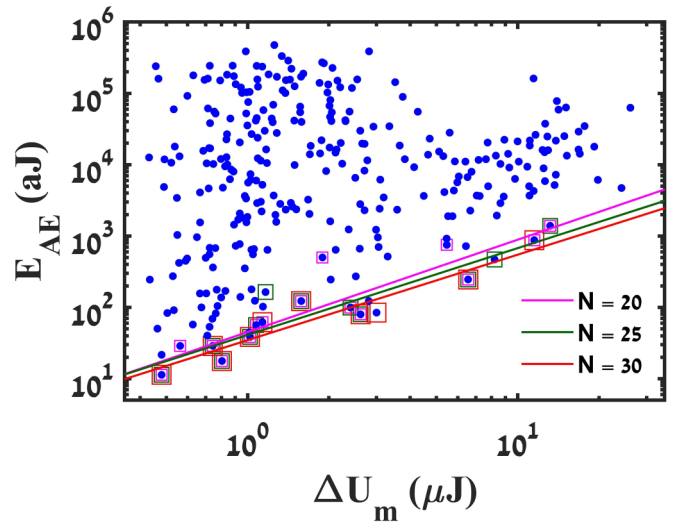


FIG. 5. AE energy vs mechanical energy drops ΔU_m (blue points). The data points marked by squares represent the minimal values of E_{AE} within individual intervals of ΔU_m . The different colors (magenta, green, and red) correspond to division of the data into intervals with different numbers of data points within each interval ($N = 20, 25,$ and $30,$ respectively). Least-squares fittings of Eq. (3) to the minimal data points correspond to solid lines.

events, such as nucleation of a microscale step on the twin boundary or a formation of a needle twin (domain) ahead of the twin boundary [23]. Such events commonly occur during a global motion of the twin boundary that is associated with a macroscale stress drop, but they can also occur during time intervals at which there is no such motion.

The observation that almost all stress drops were accompanied by one dominant AE signal motivates the analysis of the relationship between E_{AE} and ΔU_m , as plotted in Fig. 5 on a log-log plot. Evidently, the values of E_{AE} that correspond to the same ΔU_m are scattered over several orders of magnitude. Nevertheless, it is observed that the minimal values of E_{AE} within each interval of ΔU_m increase as ΔU_m increases, i.e., there is a lower bound (E_{LB}) for E_{AE} values that is an increasing function of ΔU_m .

To test that the lower bound is not generated by a sampling effect (there are more data points at small values of ΔU_m and in accordance a higher probability to find small values of E_{AE}), we performed the following procedure. First, we divided the whole data set into intervals of ΔU_m , such that within each interval there is a given number N of data points (the size of the ΔU_m intervals is not fixed). Next, we found the point with a minimal value of E_{AE} within each interval (marked in Fig. 5). Then, we fitted the function

$$E_{\text{LB}} = C \cdot \Delta U_m^z, \quad (3)$$

which appears as a straight line in the log-log plot presented in Fig. 5, to the set of data points with minimal values of E_{AE} . We repeated the same procedure for $N = 20, 25,$ and $30,$ and obtained the results presented in Fig. 5. The best fitted values of z for groups of $N = 20, 25,$ and 30 data points were $z = 1.29, 1.22,$ and $1.20,$ respectively. Thus, the sampling effect on the lower bound is minor. The obtained value of $z \approx 1.24$

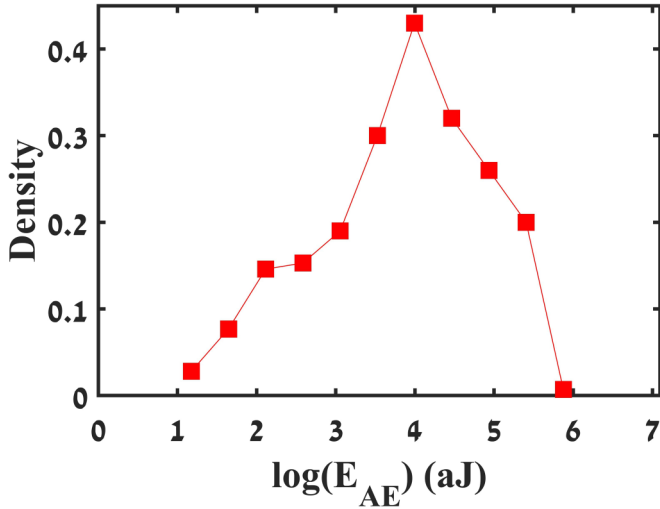


FIG. 6. PDF distribution of E_{AE} signals that were emitted during stress drop events.

(the average of the three z values) indicates that the relation between E_{LB} and ΔU_m is close to linear.

The PDF distribution of the energy of AE signals that were emitted during stress drops, i.e., the 305 data points presented in Fig. 5, is shown in Fig. 6. Note that the population that is analyzed in this figure represents 1.5% of all AE signals with an energy larger than 10 aJ. Figure 6 presents a PDF that is centered about a peak that represents a most probable (characteristic) value of the AE energy. This behavior is in contrast with the corresponding CCDF that includes all AE signals that were presented in Fig. 3. Comparison of Figs. 3 and 6 shows that the physical behavior of AE events that are emitted during detectable stress drops is significantly different from the behavior of all other AE events.

The well-defined relation between E_{LB} and ΔU_m implies that for each AE signal there are two sources that contribute to E_{AE} . One source contributes a well-defined amount of acoustic energy, E_{LB} , that is directly related to ΔU_m through Eq. (3). The other source contributes an additional energy $\Delta E = E_{AE} - E_{LB}$ that varies over several orders of magnitude, regardless of the value of ΔU_m .

The distribution of ΔE is presented in Fig. 7(a). A segment of the CCDF that displays a power law is observed for ΔE in the range of 15–500 aJ, as demonstrated by the dashed black line. We can fit a distribution function of the form

$$P(\Delta E) \sim \Delta E^{-\beta} \exp\left[-\frac{\Delta E}{\Delta E_{\text{cutoff}}}\right] \quad (4)$$

to these data by means of the ML method, provided $\beta = 1.4 \pm 0.1$. Another method for validating the power-law behavior of ΔE is by plotting the exponent β (fitted by the ML method) as a function of a varying lower cutoff ΔE_{min} , as presented in Fig. 7(b). In this method, the exponent is estimated by the plateau as indicated by the red line (see, e.g., Refs. [40,42]). According to this analysis, a value of $\beta = 1.45 \pm 0.05$ fits the results in the range of $\Delta E = 15\text{--}600$ aJ, in agreement with the black dashed line that is marked in Fig. 7(a). The results of Fig. 7 indicate that the process that contributes to ΔE can be assumed to be close to a dynamic critical state.

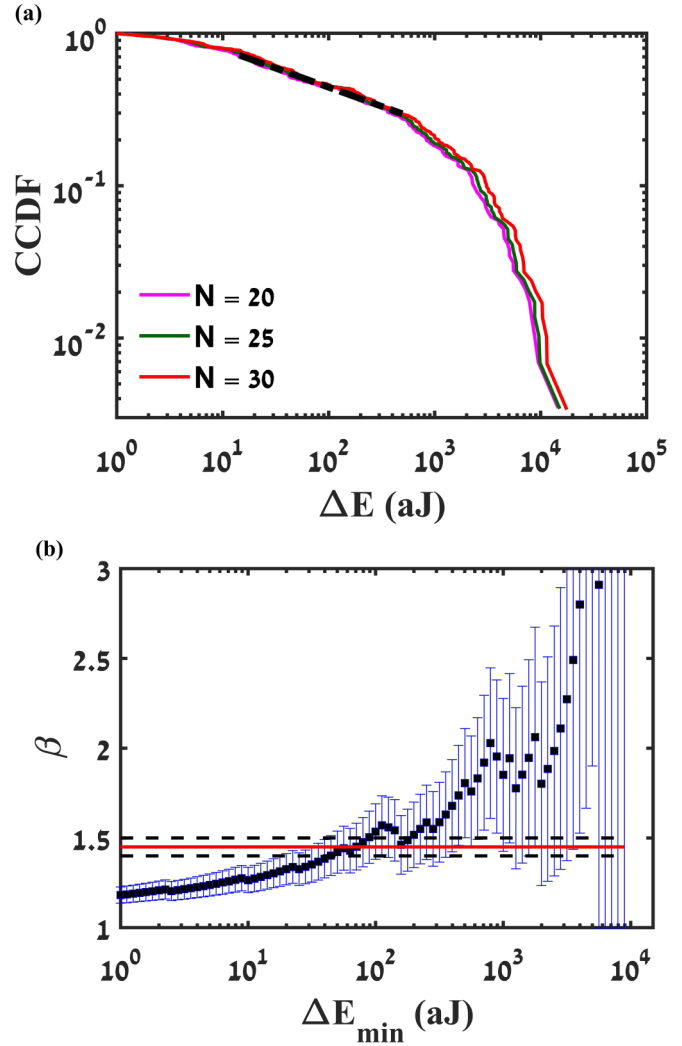


FIG. 7. (a) CCDF curves of ΔE defined with respect to the lower bounds obtained for $N = 20, 25,$ and 30 data points (see Fig. 5). (b) The power-law exponent β as a function of a varying lower cutoff ΔE_{min} for the data with $N = 20$. The red line indicates a value of $\beta = 1.45$. The stripe between the dashed black lines represents an error of ± 0.05 and fits the data in the range of $\Delta E = 15\text{--}600$ aJ.

IV. DISCUSSION

In this section, we present a possible explanation for the results presented in Figs. 5–7 and for the distinction between the two different contributions to E_{AE} . We recall that the distribution of E_{AE} is affected by the distributions of $\varepsilon_T \cdot \Delta V$ and τ , while the distribution of ΔU_m is affected only by the distribution of $\varepsilon_T \cdot \Delta V$. We suggest that the contribution represented by $E_{LB}(\Delta U_m)$ is associated with global (macroscale) stress drops that are characterized by large ΔV and τ . During such a class of events, a twin boundary that crosses the entire crystal width and has an area of $A \cong 10 \text{ mm}^2$ propagates a distance $\Delta x = (A \cdot \Delta \sigma)/(k\varepsilon_T)$ [16,23], which according to our results is in the range of 2–80 μm . The volume $\Delta V = A \cdot \Delta x$ that undergoes this twinning transformation is in the range of $\Delta V_{\text{macro}} = 0.02\text{--}0.8 \text{ mm}^3$, and the energy that is released during the event ΔU_m is larger by several orders of magnitude than E_{AE} . Such a macroscopic event generates a wide band

of acoustic waves, most of them with frequencies that are related to the duration of the stress drop (τ in the millisecond timescale) and are much lower than the frequency range detected by the AE measurement system. Thus, $E_{LB}(\Delta U_m)$ represents a small but well-defined part of the energy that is released during the stress drop.

The additional contribution, ΔE , is distributed close to a power-law distribution [Fig. 7(a)] similar to the distribution of all AE signals (Fig. 3). The exponents of the distribution of all AE signals ($\varepsilon = 1.5$) and the distribution of ΔE ($\beta \cong 1.4$) are also in good agreement (within the analyses errors). We recall that 99.8% of all AE signals that are analyzed in Fig. 3 occurred at time intervals during which there was no stress drop, i.e., no macroscale motion of the twin boundary as described above. Therefore, we suggest that ΔE is generated by microscale events that are characterized by small values of ΔV and τ . The volume ΔV_{micro} related to such events is smaller by several orders of magnitude than ΔV_{macro} , but their characteristic time τ relates to a frequency within the bandwidth of the AE transducer. Thus, the contribution of ΔE may be comparable to or even larger than $E_{LB}(\Delta U_m)$.

The microscale events described above may be related to the local overcoming of barriers for the twin boundary motion. Examples for such events may be a nucleation of a microscale step on the twin boundary or a formation of a needle twin (domain) ahead from the twin boundary [23]. Such events can occur during time intervals at which there is no macroscale motion of twin boundaries. Nevertheless, they are expected to occur at a higher rate and intensity during a macroscale motion of the twin boundary or immediately before it. Indeed, our results show that the probability of finding an AE event during a stress drop is ~ 100 times larger than between stress drops.

V. CONCLUSIONS

Synchronized measurements of stress drops and AE with high temporal resolution revealed that during the strain induced motion of a single twin boundary in a Ni-Mn-Ga shape memory alloy 94% of the stress drop events were accompanied by a single dominant AE signal. On the other hand,

99.8% of the AE signals were emitted during time intervals at which there was no detectable stress drop event. The CCDF of the mechanical energy drops ΔU_m displayed a combination of a power-law distribution at small values and a normal distribution at large values. The CCDF of the energy of all AE signals, as well as of AE signals that were not associated with a stress drop, displayed a power-law distribution over five orders of magnitude. On the other hand, the distribution of the energy of AE signals that were emitted during detectable stress drops was centered about a peak that represents a most probable value.

The reason for the different distribution of AE signals that were emitted during stress drops is the existence of a lower bound that is approximately a linear function of the mechanical energy drops. We suggest an explanation, according to which the lower bound of the AE energy is associated with the macroscopic stress changes. These events release a large amount of energy but only a small part of it is transformed to acoustic waves in the frequency range detected by the AE measurement system. An additional contribution to the AE energy, ΔE , is generated by local microscopic events, such as the overcoming of energy barriers for twin boundary motion. These events release a smaller amount of energy, but occur at the microscale timescale, and therefore a significant part of this energy is transformed to acoustic waves in the detected frequency range. We show that the distribution of ΔE is very close to a power law, which implies that the source for this energy, i.e., local microscopic events, is similar (or the same) to the source of AE signals that were not associated with a stress drop. This means that local microscopic events can also occur during time intervals at which there is no global motion of the twin boundary.

ACKNOWLEDGMENTS

This research was supported by the Israel Science Foundation (Grant No. 1268/14) and Ministerio de Economía y Competitividad, Spain (Grant No. MAT2016-75823-R).

-
- [1] H. M. Jaeger, C. H. Liu, and S. R. Nagel, *Phys. Rev. Lett.* **62**, 40 (1989).
 - [2] V. Navas-Portella, Á. Corral, and E. Vives, *Phys. Rev. E* **94**, 033005 (2016).
 - [3] J. Antonaglia, W. J. Wright, X. Gu, R. R. Byer, T. C. Hufnagel, M. LeBlanc, J. T. Uhl, and K. A. Dahmen, *Phys. Rev. Lett.* **112**, 155501 (2014).
 - [4] R. J. Harrison and E. K. H. Salje, *Appl. Phys. Lett.* **99**, 151915 (2011).
 - [5] D. Soto-Parra, X. Zhang, S. Cao, E. Vives, E. K. H. Salje, and A. Planes, *Phys. Rev. E* **91**, 060401(R) (2015).
 - [6] H. Kawamura, T. Hatano, N. Kato, S. Biswas, and B. K. Chakrabarti, *Rev. Mod. Phys.* **84**, 839 (2012).
 - [7] J. Davidsen, S. Stanchits, and G. Dresen, *Phys. Rev. Lett.* **98**, 125502 (2007).
 - [8] E. K. H. Salje and K. A. Dahmen, *Annu. Rev. Condens. Matter Phys.* **5**, 233 (2014).
 - [9] J. P. Sethna, K. A. Dahmen, and C. R. Myers, *Nature (London)* **410**, 242 (2001).
 - [10] A. Portevin and F. Le Chatelier, *C. R. Hebd. Seances Acad. Sci.* **176**, 507 (1923).
 - [11] J. Baró, Á. Corral, X. Illa, A. Planes, E. K. H. Salje, W. Schranz, D. E. Soto-Parra, and E. Vives, *Phys. Rev. Lett.* **110**, 088702 (2013).
 - [12] P. Bak, C. Tang, and K. Wiesenfeld, *Phys. Rev. Lett.* **59**, 381 (1987).
 - [13] Z. Olami, H. J. S. Feder, and K. Christensen, *Phys. Rev. Lett.* **68**, 1244 (1992).
 - [14] F.-J. Pérez-Reche, L. Truskinovsky, and G. Zanzotto, *Phys. Rev. Lett.* **101**, 230601 (2008).
 - [15] M. C. Gallardo, J. Manchado, F. J. Romero, J. del Cerro, E. K. H. Salje, A. Planes, E. Vives, R. Romero, and M. Stipicich, *Phys. Rev. B* **81**, 174102 (2010).

- [16] E. Faran, E. K. H. Salje, and D. Shilo, *Appl. Phys. Lett.* **107**, 071902 (2015).
- [17] E. Faran, H. Seiner, M. Landa, and D. Shilo, *Appl. Phys. Lett.* **107**, 171601 (2015).
- [18] M. A. Lebyodkin, N. P. Kobelev, Y. Bougherira, D. Entemeyer, C. Fressengeas, V. S. Gornakov, T. A. Lebedkina, and I. V. Shashkov, *Acta Mater.* **60**, 3729 (2012).
- [19] T. A. Lebedkina, Y. Bougherira, D. Entemeyer, M. A. Lebyodkin, and I. V. Shashkov, *Scr. Mater.* **148**, 47 (2018).
- [20] T. A. Lebedkina, D. A. Zhemchuzhnikova, and M. A. Lebyodkin, *Phys. Rev. E* **97**, 013001 (2018).
- [21] S. Puchberger, V. Soprunyuk, W. Schranz, A. Tröster, K. Roleder, A. Majchrowski, M. A. Carpenter, and E. K. H. Salje, *APL Mater.* **5**, 046102 (2017).
- [22] F. J. Romero, J. Manchado, J. M. Martín-Olalla, M. C. Gallardo, and E. K. H. Salje, *Appl. Phys. Lett.* **99**, 011906 (2011).
- [23] E. Faran and D. Shilo, in *Avalanches in Functional Materials and Geophysics*, edited by E. K. H. Salje, A. Saxena, and A. Planes (Springer International Publishing, Cham, 2017), pp. 167–198.
- [24] A. Planes, L. Mañosa, and E. Vives, *J. Alloys Compd.* **577**, Supplement 1, S699 (2013).
- [25] C. H. Scholz, *The Mechanics of Earthquakes and Faulting*, 2nd ed. (Cambridge University, Cambridge, England, 2002).
- [26] H. Kanamori and E. E. Brodsky, *Rep. Prog. Phys.* **67**, 1429 (2004).
- [27] H. Kanamori, *J. Geophys. Res.* **82**, 2981 (1977).
- [28] H. Kanamori, *Nature (London)* **271**, 411 (1978).
- [29] N. Zreihan, E. Faran, E. Vives, A. Planes, and D. Shilo, *Phys. Rev. B* **97**, 014103 (2018).
- [30] L. Straka, O. Heczko, H. Seiner, N. Lanska, J. Drahoukoupil, A. Soroka, S. Fähler, H. Hänninen, and A. Sozinov, *Acta Mater.* **59**, 7450 (2011).
- [31] H. Seiner, L. Straka, and O. Heczko, *J. Mech. Phys. Solids* **64**, 198 (2014).
- [32] L. Straka, H. Hänninen, and O. Heczko, *Appl. Phys. Lett.* **98**, 141902 (2011).
- [33] E. Faran and D. Shilo, *Appl. Phys. Lett.* **100**, 151901 (2012).
- [34] E. Faran and D. Shilo, *J. Mech. Phys. Solids* **61**, 726 (2013).
- [35] E. Faran and D. Shilo, *Mater. Sci. Technol.* **30**, 1545 (2014).
- [36] A. Clauset, C. Shalizi, and M. Newman, *SIAM Rev.* **51**, 661 (2009).
- [37] N. Glavatska, G. Mogylny, I. Glavatskiy, and V. Gavriljuk, *Scr. Mater.* **46**, 605 (2002).
- [38] L. Dai, J. Cullen, and M. Wuttig, *J. Appl. Phys.* **95**, 6957 (2004).
- [39] L. Mañosa, A. González-Comas, E. Obradó, A. Planes, V. A. Chernenko, V. V. Kokorin, and E. Cesari, *Phys. Rev. B* **55**, 11068 (1997).
- [40] H. Bauke, *Eur. Phys. J. B* **58**, 167 (2007).
- [41] J. Baró and E. Vives, *Phys. Rev. E* **85**, 066121 (2012).
- [42] E. Vives, J. Baró, M. C. Gallardo, J.-M. Martín-Olalla, F. J. Romero, S. L. Driver, M. A. Carpenter, E. K. H. Salje, M. Stipcich, R. Romero, and A. Planes, *Phys. Rev. B* **94**, 024102 (2016).